

Dynamic Asset Allocation via Quantum Annealing

Hanjing Xu,^{1,*} Samudra Dasgupta,^{2,3,†} Alex Pothen,^{1,‡} and Arnab Banerjee^{2,§}

¹*Department of Computer Science, Purdue University, West Lafayette, IN, 47906*

²*Department of Physics, Purdue University, West Lafayette, IN, 47906*

³*Bredesen Center, University of Tennessee, Knoxville, TN, 37996*

(Dated: December 7, 2021)

Recent advancements in quantum hardware offer new approaches to solve various optimization problems that can be classically computationally expensive. We propose a hybrid algorithm to address a problem related to portfolio optimization. The algorithm converts Markowitz's Mean-Variance Model to a Quadratic Unconstrained Optimization Problem (QUBO) and incorporates expected shortfall as the risk measurement to better adapt to markets during extreme events. We compare the results from 2000Q and Advantage quantum annealers from D-Wave using real-world financial data. Both quantum annealers are able to generate portfolios more than 80% of the classical optimal solutions. We observe that experiments on assets with higher correlations tend to perform better which may help guide designing practical quantum applications in the near term.

I. INTRODUCTION

Quantum annealing offers a highly parallelized approach for optimization problems by means of quantum tunneling between a manifold of solutions and converging to the ground state. A common approach to embed the optimization problem into an Ising quantum annealer is by converting them to QUBO (Quadratic Unconstrained Binary Optimization) problems. Several examples have been explored so far in the literature, including the maximum clique problem [1], nurse scheduling problem [2] and graph coloring problem [3].

Another popular optimization problem introduced by Harry Markowitz [4] in 1952 is the portfolio optimization problem. This problem investigates how investors could use the power of diversification to optimize portfolios by minimization of risk and serves as a foundation for later models such as the Black-Litterman model [5]. The original Markowitz model uses volatility as the measure of the risk which works well most of the times, but it often fails to characterize the market during extreme events or 'shocks', e.g., the 2008 mortgage crisis which led to an abrupt collapse with the insolvency of Lehman Brothers. As a result, the financial managers instead increasingly prefer to use the expected loss when the loss has already exceeded a threshold, i.e., expected shortfall [6]. The advantages of expected shortfall over other risk measurements like volatility or Value-at-Risk are discussed in Ref. [7].

Due to the high computational complexity [8] of solving a large-scale quadratic optimization program like the portfolio optimization problem and its time-sensitive nature, numerous classical algorithms have been developed over the years to reduce the computational cost. On

the other hand, as more versatile and scalable quantum computing devices - mainly quantum annealers - enter the market, we explore application of the portfolio optimization problem on two quantum annealers that are available today.

Grant *et al.* [9] benchmarked the performance of D-Wave 2000Q on solving the Markowitz Mean-Variance Optimization Problem with a relatively small size of 20 logical qubits and randomly generated return date. In this manuscript, we take inspiration from that study and expand on their experiments but using expected shortfall as the measure of the risk on which the model is optimized. We design a hybrid algorithm that uses the Markowitz's model as a quantum annealing subroutine to obtain the optimal portfolio based on expected shortfall. Based on experiments consisting of both real-world ETF and currency data, we were able to show a solubility of the QUBO model and explore its performance on both generations of quantum annealers offered by D-Wave in up to 115 logical qubits.

In this manuscript, we discuss a method of formulating the continuous variable Markowitz model as a QUBO problem and develop the use of expected shortfall as a metric to evaluate the risk of the portfolio in a hybrid manner. We provide experimental results on both the Advantage (Pegasus topology) and 2000Q (Chimera topology) D-Wave quantum annealers. The results are generally close to the optimal portfolios in terms of final returns and Sharpe ratios obtained by classical methods. We observe that more correlated assets yield better performance on the quantum annealers, which may provide a use case for such devices in real application in the near term. We also assess the performance impact of concatenating one of the constraints to the objective function which leads to one fewer Lagrangian multiplier.

The paper is structured as follows. Sec. II states the background on quantum annealing algorithms, hardware and relevant research, Sec. III lays out the algorithm and argues its correctness and Sec. IV discusses the experimental results on both D-Wave 2000Q and Advantage systems. Sec. V concludes the paper with a few future

* xu675@purdue.edu

† samudra.dasgupta@gmail.com

‡ apothen@purdue.edu

§ arnabb@purdue.edu

research directions.

II. BACKGROUND

A. Quantum Annealing and Ising Models

Quantum annealing is a physical implementation of adiabatic quantum computation [10] with a focus on obtaining the ground state of an objective function (i.e., a Hamiltonian) by minimizing the energy of Ising models:

$$E(s) = \sum_i h_i s_i + \sum_{i,j} J_{ij} s_i s_j, \quad s_i \in \{-1, 1\}, \quad (1)$$

where s is the classical spin variable, h is the external longitudinal magnetic field strength vector and the matrix J represents the coupler interactions. This problem is NP-hard [11] for arbitrary h and J .

A Quadratic Unconstrained Optimization Problem (QUBO) of the form

$$Q(x) = \sum_i h_i x_i + \sum_{i,j} J_{ij} x_i x_j, \quad x_i \in \{0, 1\} \quad (2)$$

can be converted to an Ising problem by a one-to-one mapping of the variables: $x_i = \frac{1+s_i}{2}$. We will use QUBO for the rest of the paper but it is worth noting that quantum annealers from D-Wave require the QUBOs to be transformed into Ising models before running on the processor.

Given a standard binary optimization problem with a linear or quadratic objective function,

$$\begin{aligned} \min_x \quad & f(x) \\ \text{s.t.} \quad & Ax = b \\ & x \in \{0, 1\}^n, \end{aligned} \quad (3)$$

we can rewrite it as a QUBO

$$Q(s) = f(x) + \lambda(Ax - b)^T(Ax - b) \quad (4)$$

to be minimized by quantum annealers. We will discuss how to convert the Markowitz optimization problem to have continuous variables in Section III A.

B. D-Wave Quantum Annealer

Here we start by discussing the latest quantum annealing technologies offered by D-Wave as we will see, the solubility of the problem is deeply dependent on the offered architecture. D-Wave quantum annealers are specifically designed to solve Ising problems natively. Currently two types of quantum annealers are offered by D-Wave: ‘2000Q’ processor with Chimera topology and ‘Advantage’ processor with Pegasus topology. The later one was made publicly available in 2020 and it has more

qubits (5760 vs. 2048) and better connectivity. The qubits in the Chimera topology have 5 couplers per qubit while in the Pegasus topology they have 15 couplers per qubit [12]. It is not always possible to formulate an optimization problem to match the Chimera or Pegasus topologies exactly. Therefore minor embedding are necessary to map the problems to D-Wave processors. Such embeddings usually require the users to map multiple physical qubits to one logical variable which significantly reduces the total size of the problems that can be solved in the quantum annealers.

Furthermore, it is advisable to have uniform chain lengths - numbers of qubits representing a single variable - and uniform number of physical couplers for each logical coupler for more predictable chain dynamics during the anneal [13]. Algorithms in [14] detail such procedures for cliques which is the underlying logical graph for the portfolio optimization problem. A full-yield 2000Q processor can map up to 64 logical variables and an Advantage processor can map around 180 logical variables. A comparison between the embedding of the two topologies is shown in Figure 1. In the experiments we use the *find_clique_embedding* function from *dwave-system* to map fully-connected graphs to either Chimera or Pegasus topology.

C. Previous Work

Rosenberg *et al.* [15] solved multi-period portfolio optimization problem using D-Wave’s quantum annealer:

$$\begin{aligned} \max_w \quad & \sum_{t=1}^T (\mu_t^T w_t - \frac{\gamma}{2} w_t^T \Sigma_t w_t - \Delta w_t^T \Lambda_t \Delta w_t + \Delta w_t^T \Lambda'_t \Delta w_t) \\ \text{s.t.} \quad & \sum_{n=1}^N w_{nt} = K, \forall t, \\ & w_{nt} \leq K', \forall t, \forall n. \end{aligned} \quad (5)$$

Eq. (5) seeks to maximize returns considering the portfolio variance and transaction costs. The sum of asset holdings is constrained by K and the maximum allowed holdings of each asset is K' . For small problems ranging from 12 to 584 variables, D-Wave’s 512 and 1152-qubit systems were able to find optimal solutions with high probability.

Venturelli and Kondratyev [16] focused on the following QUBO where the task is to select M assets from a pool of N assets:

$$\sum_{i=1}^N a_i q_i + \sum_{i=1}^N \sum_{j=i+1}^N b_{ij} q_i q_j + P \left(M - \sum_{i=1}^N q_i \right) \quad (6)$$

Coefficients a_i indicates attractiveness of the i -th asset and b_{ij} is the pairwise diversification penalties (positive) or rewards (negative). q_i is set to 1 if the i -th asset is selected and P scales the constraint to make sure it is

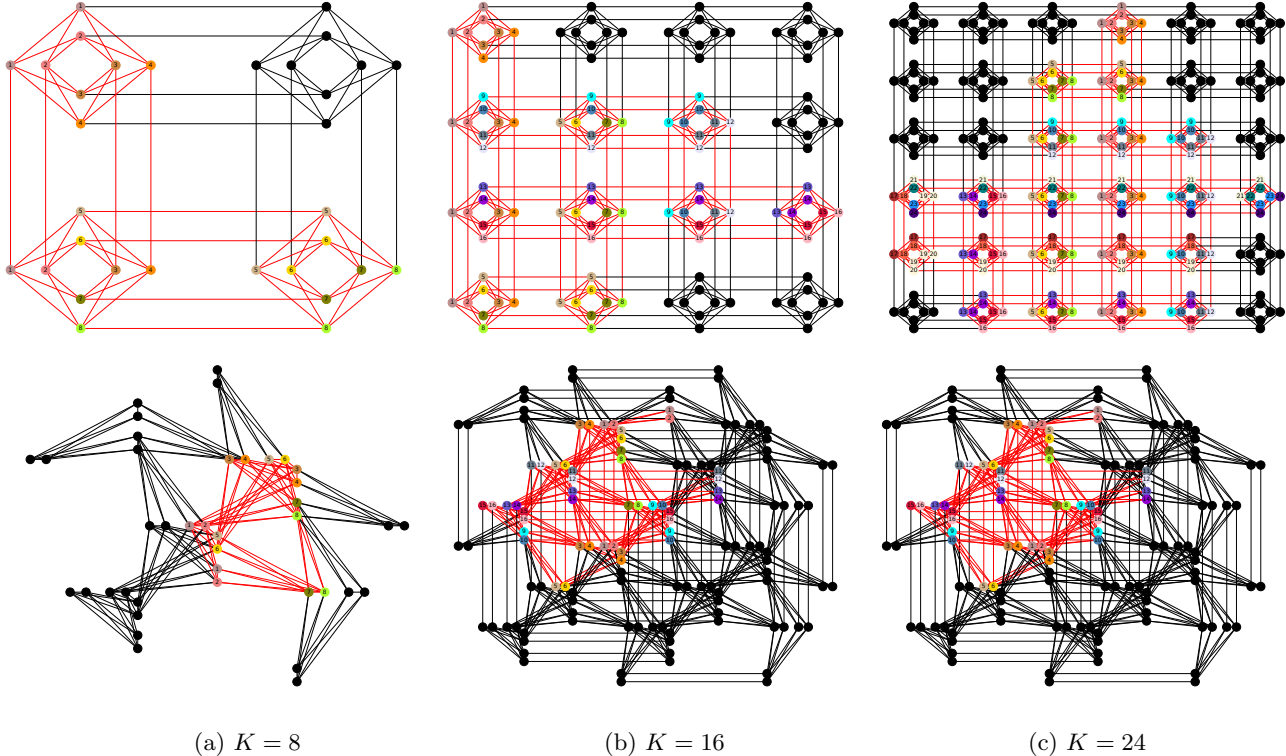


FIG. 1. A comparison between minor embeddings on Chimera and Pegasus lattices for cliques (fully connected graphs) of different sizes. The vertices with the same color or label represent the same logical variable in Eq. (1). Each Chimera cell is a 4 by 4 complete bipartite graph ($K_{4,4}$) with 4 additional edges connecting neighboring cells. Each Pegasus cell has 24 qubits which include 3 $K_{4,4}$ graphs as in the Chimera cell and $K_{2,4}$ edges connecting them. To minor embed cliques of 8 vertices ($K = 8$), the chain length on the Chimera lattice is 3 while on the Pegasus lattice it is 2. With $K = 16$, the chain lengths are 5 and 2-3, respectively, and with $K = 24$, they are 7 and 3-4, respectively. This shows that Pegasus processor scales better for larger clique problems, which may lead to better performance.

satisfied during the annealing process. The authors also explore the benefits of reverse annealing on D-Wave systems and report one to three orders of magnitude speed-up in time-to-solution.

The problem considered by Phillipson and Bhatia [17] is similar to the Markowitz Optimization problem but with binary variables indicating asset selections instead of real weights. The authors report comparable results from D-Wave's hybrid solver to other state of the art classical algorithms and solvers including simulated annealing, genetic algorithm, linear programs (Gurobi with Branch and Bound Algorithm) and local search.

Grant *et al.* [9] benchmark the Markowitz Optimization problem on D-Wave 2000Q processor with real weight variables and uniform price data and explore how embeddings, spin reversal and reverse annealing affect the success probability. The novel contribution in our paper is to follow the general QUBO formulation in [9], and benchmark with real-world ETF and currency data. Additionally, we present the results on the newly-available Advantage processor and experiment on problems with 30 and up to 115 logical spins, up from 20 in [9].

III. METHODS

A. Markowitz Model in Mean-Shortfall Optimization and its QUBO Formulation

The expected shortfall is defined as the expected return on the portfolio in the $\alpha\%$ worse cases. It is possible to write the mean-shortfall optimization problem as a linear program [18] but it requires adding $T + 1$ variables and $2T$ constraints where T is the number of assets. However, under the assumption that the assets' historical returns follow a Gaussian distribution we can approximate the expected shortfall by:

$$\text{ES}_\alpha(P) = \mu + \sigma \frac{\phi(\Phi^{-1}(\alpha))}{1 - \alpha}, \quad (7)$$

where μ is the mean of the return data, σ is the volatility of the portfolio, and $\phi(x)$ and $\Phi(x)$ are the Gaussian probability distribution and cumulative distribution function, respectively [19]. It is clear that the expected shortfall has positive correlation with the volatility and in turn, the variance of the portfolio.

Thus instead of minimizing the expected shortfall directly in the optimization program, we use the Markowitz Model [4] to find a portfolio with minimum volatility given the target return is met:

$$\begin{aligned} \min_w \quad & w^T C_t w \\ \text{s.t.} \quad & \mu_t^T w = p, \\ & \sum w_i = 1, w_i \geq 0 \quad \forall i. \end{aligned} \quad (8)$$

Here w is the weight vector, C_t is the co-variance matrix of the assets' returns during time window t , R is the historical return data, $\mu_t = \text{mean}(R)$ is the mean return vector of time window t , and p is the target return. The constraint $\mu_t^T w = p$ ensures that the target return is met, $\sum w = 1$ indicates we want to invest all of the resources, and $w \geq 0$ means short selling is not allowed. With all the constraints satisfied, we minimize $w^T C_t w$, i.e., the variance of the portfolio.

To convert Eq. (8) to a QUBO, first we write it as an unconstrained optimization program with Lagrangian multipliers λ_1, λ_2 and λ_3 :

$$\mathcal{L} = \left(\sum_i^n \sum_j^n C_{i,j} w_i w_j \right) + \lambda_1 \left(\sum_i^n \mu_{t,i} w_i - p \right)^2 + \lambda_2 \left(\sum_i^n w_i - 1 \right)^2 \quad (9)$$

where λ_1 and λ_2 scale the constraint penalties. It is also equivalent to

$$\begin{aligned} \mathcal{L} = & \left(\sum_i^n \sum_j^n C_{i,j} w_i w_j \right) + \\ & \lambda_1 \left[\left(\sum_i^n \mu_{t,i} w_i \right)^2 - 2p \sum_i^n \mu_{t,i} w_i \right] \\ & + \lambda_2 \left[\left(\sum_i^n w_i \right)^2 - 2 \sum_i^n w_i \right] \end{aligned} \quad (10)$$

after expanding the squared terms and eliminating the constants. When the constraints are satisfied exactly, we have

$$\lambda_1 \left[\left(\sum_i^n \mu_{t,i} w_i \right)^2 - 2p \sum_i^n \mu_{t,i} w_i \right] = -\lambda_1 p^2, \quad (11)$$

and

$$\lambda_2 \left[\left(\sum_i^n w_i \right)^2 - 2 \sum_i^n w_i \right] = -\lambda_2. \quad (12)$$

We use k binary variables $x_1 \dots x_k \in \{0, 1\}$ to approximate the continuous variable w in Eq. (8)

$$w_i = \sum_{a=1}^k 2^{-a} x_i. \quad (13)$$

The larger k is, the more precision w_i has. However, smaller k also widens the differences between the coupler strengths - J terms in Eq. (2). Although the coupler strengths for D-Wave annealers can be set at any double-precision floating point number between -1 and 1 , errors in precision pose a challenge to D-Wave annealers due to integrated control errors (ICE) [20]. In reality D-Wave processors solve a slightly modified version of Eq. (2),

$$Q^\delta(s) = \sum_i (h_i + \delta h_i(s)) x_i + \sum_{i,j} (J_{ij} + \delta J_{ij}(s)) x_i x_j. \quad (14)$$

Here δh and δJ are time-dependent and [21] shows an example of their distribution during the anneal for a 2000Q processor.

In our experiments, we set $k = 5$ which achieves a good enough approximation on the weights while keeping all coupler strengths close. For larger k we will risk the errors dominating the coupler coefficients, rendering those additional qubits unreliable. We also set λ_1 to p^{-2} and λ_2 to 1 such that the QUBO will have a theoretical minimum objective value of $-2 + \lambda_3 \left(\sum_i \sum_j C_{i,j} w_i w_j \right)$ when the constraints are satisfied exactly by Eq. (11) and Eq. (12).

Substituting Eq. (13) in to Eq. (10), we have the final binary optimization formalism

$$\begin{aligned} f(x) = & \left[\left(\sum_i^n \sum_a^k \mu_{t,i} 2^{-a} x_i \right)^2 - 2p \sum_i^n \sum_a^k \mu_{t,i} 2^{-a} x_i \right] \\ & + p^{-2} \left[\left(\sum_i^n \sum_a^k 2^{-a} x_i \right)^2 - 2 \sum_i^n \sum_a^k 2^{-a} x_i \right] \\ & + \lambda_3 \left(\sum_i^n \sum_j^n \sum_a^k \sum_b^k C_{i,j} 2^{-a-b} x_i x_j \right), \end{aligned} \quad (15)$$

which is quantum-annealable as it only has linear and quadratic interactions.

B. Quantum-Classical Algorithm for Portfolio Optimization

Since expected shortfall cannot be expressed as a quadratic formulation exactly, we opt to use it as a convergence criterion instead of including it in the optimization problem directly. We use a hybrid approach where we optimize the portfolio weights and the constraints on

Algorithm 1: Expected Shortfall based Dynamic Asset Allocation during t .

Input: $\mu_t, R_t, \sigma_{ref}, \sigma_{ref,t}, ES_{ref}$
Output: w

Let $p = \text{mean}(\mu_t)$; ▷ Initialize the target return
 Let $EST_t = \frac{\sigma_{ref}}{\sigma_{ref,t}} ES_{ref}$; ▷ Initialize the target expected shortfall
 Let $C_t = \text{cov}(R_t)$; ▷ Compute the co-variance matrix from the returns
while *True* **do**
 | **if** $p > \text{max}(\mu_t)$ **then**
 | | Return $\mathbf{0}$; ▷ Return constraint cannot be satisfied
 | | Solve Eq. (10) for w ;
 | | Let EST be the mean of the lowest $\alpha\%$ values of $w^T R_t$; ▷ Compute the expected shortfall from the asset weights
 | | **if** $\frac{|EST|}{|EST_t|} > 1 + \epsilon$ **then**
 | | | Let $p = p(1 - \delta)$; ▷ Decrease target return for lower risks
 | | | **else if** $\frac{|EST|}{|EST_t|} < 1 - \epsilon$ **then**
 | | | | Let $p = p(1 + \delta)$; ▷ Increase target return as there is room for more risks
 | | | **else**
 | | | | Return w ;
end

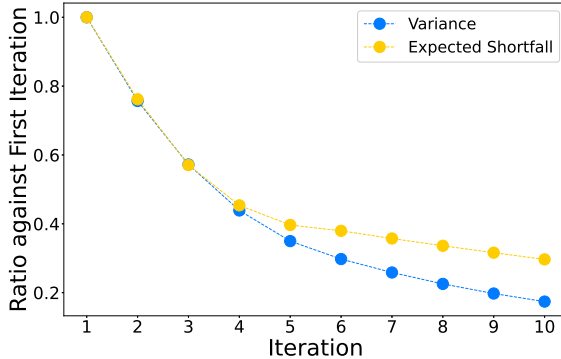


FIG. 2. Y-axis tracks the ratio between the variance and expected shortfall in later iterations against their respective values in the first iteration. The expected shortfall decrease at different rates from the variance but each iteration in the algorithm is guaranteed to make progress towards the target expected shortfall, which ensures convergence.

the target return, p , in two different steps – the optimization of the weights are performed in a quantum annealer, while the adjustments of p were evaluated classically based on the quantum annealing results.

Here σ is the volatility of the reference asset's returns during time window t or 2008, α is the risk level parameter, EST_t is the target expected shortfall at time window t , EST is the expected shortfall for the computed portfolio during the optimization process at time window t , ϵ is the error tolerance parameter, and δ is the momentum parameter which should be adjusted dynamically.

In the previous section we explain the usage of the Markowitz Model in a mean-shortfall problem. Fig. 2 is one example from Algorithm 1 solved with an exact solver.

IV. RESULTS

A. Test Input and Annealer Parameters

We pick the top-six ETFs by trading volumes, EEM, QQQ, SPY, SLV, SQQQ and XLF, and six major currencies' USD exchange rates, AUD, EUR, GBP, CNY, INR and JPY, for most of the tests below and extracted their return data from Yahoo Finance. The reference assets for ETF and currency tests are SPY and EUR, respectively. For the final tests which use 12 and 23 assets respectively, we choose the top ETFs by trading volumes again.

We can control a range of annealer parameters that may impact the solution quality in various degrees. Specifically, we set the number of spin reversal transforms [22] to 100 and readout thermalization to 100 μ s as suggested in [23, 24]. We set the anneal time at 1 μ s as longer anneal time sees no statistically significant improvements to the solutions similarly reported in [9]. Results from 2000Q and Advantage processors are both included in the following sections. Additionally, we report the results from D-Wave's post processing utility on 2000Q processors, which decomposes the underlying graph induced by the QUBO into several low tree-width subgraphs [25] then solve them exactly using belief propagation on junction trees [26].

We sample all QUBOs 30,000 times with both D-Wave backends and report the samples with lowest energy each time. Fig. 3 shows an example distribution of the samples.

B. Embedding Comparison on D-Wave Annealers

As discussed in Section II B, D-Wave quantum annealers require the problems to be minor embedded to the

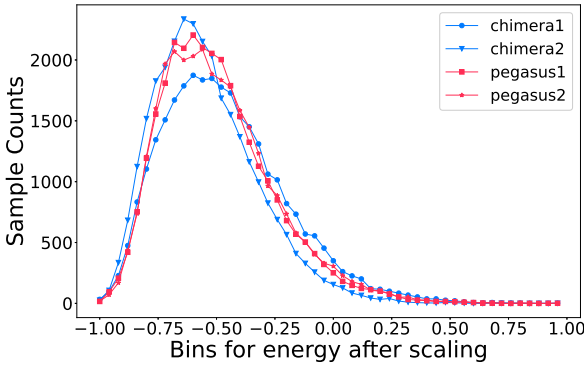


FIG. 3. The distribution of the samples for 4 different QUBOs with both D-Wave backends. Each QUBO is sampled 30,000 times and the energy of the samples is scaled to be between (-1,1). We divide the energy range into 50 equally-spaced bins and count the number of samples in each bin. All four samples exhibit the Poisson distribution, and thus we only report the samples with the lowest energy for the experiments in this section.

Chimera or Pegasus topology. For small problems this means there may be multiple valid embeddings and in this section we will measure how different embeddings can make an impact on the solution quality.

We compute 4 different embeddings that use different subgraphs from both Chimera and Pegasus topology and sample the same QUBO - first iteration of Algorithm 1 on the ETFs from December, 19 to May, 20 - 10 times with 10,000 samples each. We then pick the best solutions in terms of QUBO energy from all 10 sample sets for each embedding and obtain their average and minimum values. Table I represents the results as ratios against the ground energy computed by simulated annealing for better readability.

TABLE I. Embedding comparison on the 2000Q processor with 30 logical qubits or 270 physical qubits after minor embedding. The energy is defined as the objective value from Eq. (15) and is normalized against the simulated annealer. The second embedding out of these four is able to find the solution with better average and best energy.

Embedding	Average Energy	Best Energy
1	95.66%	98.78%
2	96.83%	99.66%
3	96.53%	98.37%
4	96.21%	98.49%

We can see that the impact that different embeddings make is statistically insignificant. However, it is clear that Pegasus processors have higher energy ratios than Chimera ones, which we will address next.

TABLE II. Embedding comparison on the Advantage processor with 30 logical qubits or 134 physical qubits after minor embedding. Different embeddings on the Advantage processor show no statistically significant differences.

Embedding	Average Energy	Best Energy
1	99.25%	99.89%
2	99.52%	99.94%
3	99.22%	99.95%
4	99.48%	99.89%

C. Annealing Results Comparison

We benchmark our algorithm on both simulated and quantum annealers against a classical optimization solver, namely, `cvxpy` [27]. The results are normalized against the optimal classical solution. The algorithm fails to converge on the first two currency tests on the 2000Q processor and they are reported as 0 in the chart.

With 5 qubits to represent each asset weight variable, the simulated annealing results follow the optimal solutions closely in most tests. We note that the quantum annealers produce results better than their classical counterparts in terms of returns and sharpe ratios in some cases. We also observe the currency tests generally perform better than ETF tests on both quantum annealer backends. Figure 6 shows how quantum annealers perform with respect to the average of absolute correlation coefficients over all pairs of assets in each test.

Although we acknowledge there may be other factors contributing to our observations that currency tests do better than ETF tests on quantum annealers, Fig. 6 implies that more correlated assets tend to perform better. Detailed analysis on which attributes of the assets have an impact on the quantum annealing performance and how much are the impacts requires more research in the future. A reference study from [28] used machine learning models such as decision tree and regression to predict the accuracy of D-Wave's quantum annealer on maximum clique problems.

D. Alternate QUBO Formulation For the Markowitz Model

Instead of having to optimize both λ_1 and λ_2 in Eq. (10), we can reformulate Eq. (8) to have one fewer Lagrangian multiplier:

$$\begin{aligned} \min_w \quad & w^T C_t w - q\mu_t^T w \\ \text{s.t.} \quad & \sum w = 1, \quad w \geq 0. \end{aligned} \quad (16)$$

To prove this, note that the Lagrangians for Eq. (8) and Eq. (16) are

$$\mathcal{L}_1(w, \lambda_1, \lambda_2) = w^T C_t w + \lambda_1(\mu_t^T w - p) + \lambda_2(1^T w - 1), \quad (17)$$

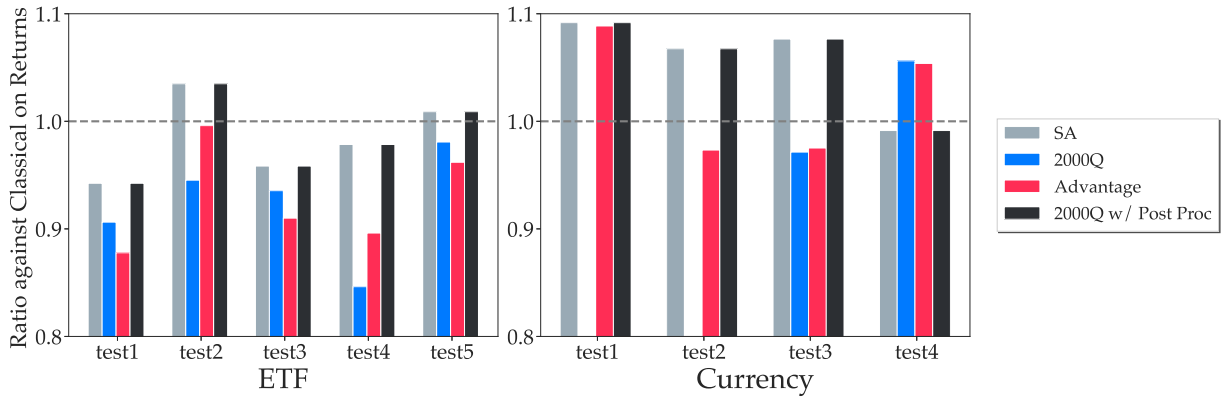


FIG. 4. The comparison of the final returns between all 4 backends. Each test uses 100 days of return data with different starting dates from 2010 to 2020. The results from 2000Q with post processing yields identical results from simulated annealing. Both 2000Q and Advantage processors are able to compute returns that are consistently more than 80% of the optimal except the two currency test cases where the algorithm fails to converge on the 2000Q.

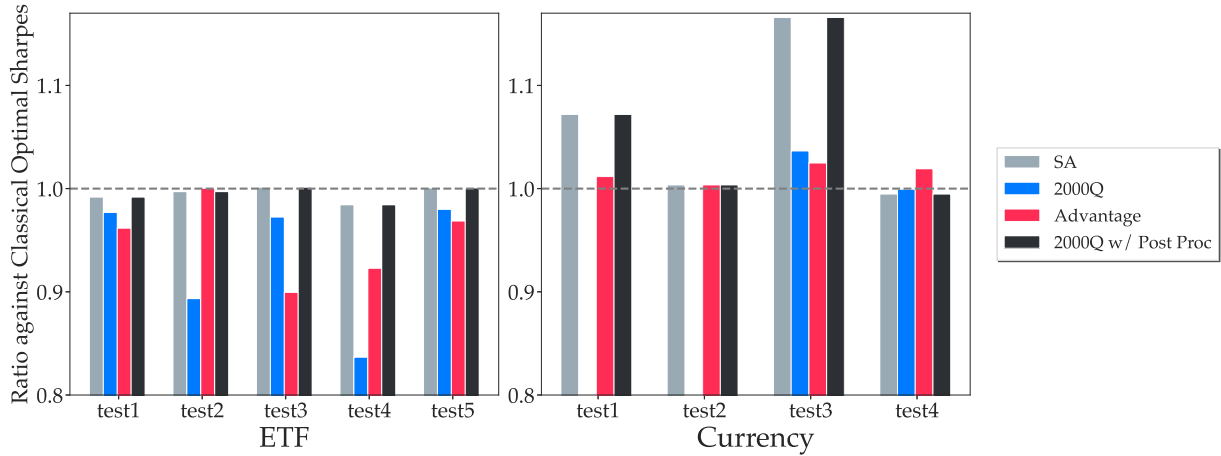


FIG. 5. The comparison of the final Sharpe ratios between all 4 backends. Sharpe ratio is calculated as return/std. The results confirm that the portfolio variance returned by the quantum processors are close to optimal results obtained from classical optimization methods, and it is effective to solve standard constrained optimization problems as a QUBO.

and

$$\mathcal{L}_2(w, \lambda_2) = w^T C_t w - q\mu_t^T w + \lambda_2(1^T w - 1). \quad (18)$$

Subtracting Eq. (18) from Eq. (17), we have

$$\mathcal{L}_1(w, \lambda_1, \lambda_2) - \mathcal{L}_2(w, \lambda_2) = (\lambda_1 - q)\mu_t^T w - \lambda_1 p, \quad (19)$$

which is a constant. Therefore Eq. (8) and Eq. (16) are equivalent and are both quantum-annealable.

However, the quantum annealing results from the alternating QUBO formulation is significantly worse than that of the original formulation. One possible explanation for the poor results is that the variance ($w^T C_t w$) and the expected return ($q\mu_t^T w$) have different scales and without the additional Lagrangian multiplier in the original QUBO formulation to regulate them, it is harder for the quantum annealers with limited accuracy to find the ground state.

E. State of The Art on D-Wave Annealers

The embeddings of the 6 asset tests on both 2000Q and Advantage processors leave plenty of unused qubits. D-Wave's clique embedding algorithm [29] suggests that we can embed a fully-connected graphs of vertex counts of 64 and 180 to full-yield 2000Q and Advantage processors, respectively. Due to the defective qubits and connectors in the currently available Advantage processor, experimentally we can embed up to 119 qubits. This means we can solve portfolio optimization problems with 12 and 23 assets natively on the D-Wave processors.

On the 12 asset test, the 2000Q processor struggles to find the ground state as its embedding chain length reaches 16 while the Advantage processor stays closely with the simulated annealing and post-processed results. However, neither quantum annealer succeeds in converging as the classical counterparts do.

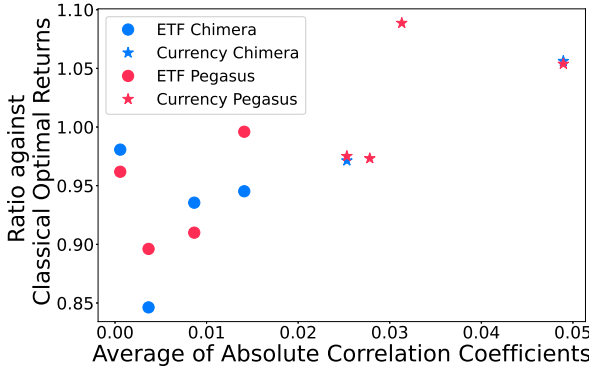


FIG. 6. Final returns obtained from both quantum annealers against the average of the absolute correlation coefficients. All currency samples in our tests have higher average correlation values than those of ETF samples.

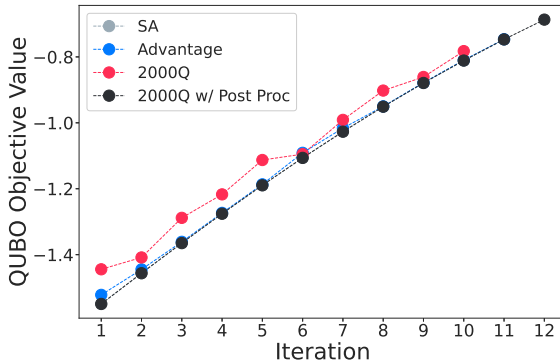


FIG. 7. The energy comparison of the 12 asset test between all 4 backends. The solutions from 2000Q deviate from the ground states by a large margin while the Advantage processor is able to keep up closely. Post processing is able to improve the 2000Q results to match simulated annealing, again.

TABLE III. Energy of Last 5 Iterations from simulated annealing and Advantage. Even though the differences in the energy are small, the results in terms of the portfolio weights vary greatly.

SA	Pegasus	difference
-1.026824759	-1.016152942	1.0393%
-0.951012554	-0.950129253	0.0928%
-0.879067674	-0.878089411	0.1112%
-0.811026432	-0.809642008	0.1707%
-0.74698612	-0.746420758	0.0757%

Comparing the last 5 iterations in terms of energy from simulated annealing and the Advantage processor shows that even the energy is hardly different, the solution quality is increasingly sensitive to the QUBO objective value that for a problem this size, a 0.1% change in the objective value leads to 30% difference in the portfolio vari-

ance. One potential reason is that solving larger problems increases the size of co-variance matrix and also the condition number. And as shown in the previous section larger condition number generally equates to worse quantum annealer performance. In this case, either the quantum annealers need to be more accurate to find the ground state or our QUBO setup needs to change to account for higher asset counts.

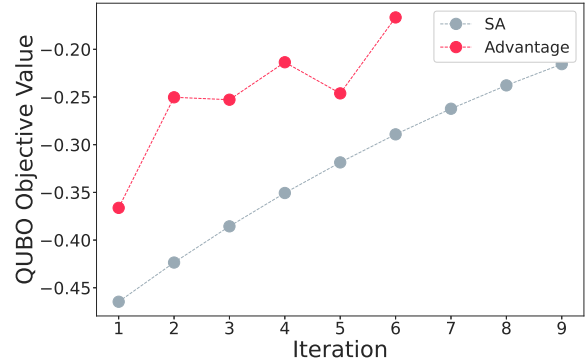


FIG. 8. The energy comparison of the 23 asset test between simulated annealing and the Advantage processor. Due to the high chain lengths of the embedding, the Advantage processor fails to either reach the ground state or get close to it in all iterations, rendering the processor incapable of solving problems of such sizes.

With the embedding chain lengths going up to 17, the Advantage processor fails to find the ground state by a large margin. Even though we can physically map a problem of this size, the results reflect the limitations of current-generation quantum annealers.

V. CONCLUSION AND FURTHER RESEARCH

As newer quantum devices are released every year it is important to design and benchmark algorithms across generations. As companies and researchers race to build the first quantum computer that can demonstrate quantum supremacy on practical problems, different classes of quantum devices have emerged: general purpose quantum computers from IBM, Google, Honeywell and etc., specialized quantum Ising machine from D-Wave and quantum-inspired digital annealer from Fujitsu. These devices have different types of restrictions on noise, qubit availability or implementable Hamiltonians, and none is perhaps at the scale needed to solve real-world problem variable sizes. Therefore hybrid algorithms are needed to incorporate these quantum computers on practical problems with reasonable size.

In this paper we have shown that it is not only possible to introduce such hybrid algorithm schemes that compute the optimal portfolios based on expected shortfall, but also highlighted where it is possible to reach a

working accuracy. We used a quantum annealers to solve a discretized version of the Markowitz Model and interlaced with a layer of classical decision making where we iteratively adjusted our problem Hamiltonian based on its result until the portfolio is within the risk threshold. The fact that both D-Wave 2000Q and Advantage quantum annealers performed reasonably well on the 6-asset tests with portfolios' Sharpe ratios to above 80% of SA values is encouraging. Also encouraging is that the the newer and more scalable Advantage processor achieved much better QUBO objective values on problems with 12 assets. Finally, we observed that both quantum annealers tended to obtain portfolios with higher returns on more correlated assets (Fig. 6), which we believe should attract future research as it may help guide the application of quantum annealing on real world applications in the near term.

Although the quantum annealers fell short on tests with more assets, we can remain optimistic about new hardware with more qubits, better connectivity and lower noise in the near future. We also acknowledged the need to design algorithms that can scale with these new hardware as we saw the portfolio's quality becomes increasingly sensitive to the QUBO objective values as we introduce more assets - results with 99.9% objective values of the optimal led to 30% more variance. Additionally, advancements in gate-model quantum computers and combinatorial optimization algorithms [30, 31] provide an-

other avenue for solving these problems.

Future research includes identifying subsets of problems that can be solved better on quantum devices as we have discussed in Sec. IV. It is also important to find an efficient way to implement inequality constraints as adding slack variables may not be the best choice in the QUBO. We also note that during specific test cases, quantum annealers outperformed classical solvers. We theorized it was possibly due to the hardware noise which allowed the quantum annealers to solve a slightly different problems as described in Eq. (14). Here the noise gave us better portfolios and exploiting this property can prove beneficial before error-corrected quantum computers are available.

ACKNOWLEDGMENTS

We like to thank Dr. Erica Grant, Dr. Andrew King, Dr. Isil Ozfidan and Dr. Travis Humble for helpful discussions. This research performed using D-Wave used resources of the Oak Ridge Leadership Computing Facility (OLCF) at the Oak Ridge National Laboratory (ORNL), which is supported by the Office of Science of the U.S. Department of Energy under Contract No. DE-AC05-00OR22725. AB and SD likes to thank the ORNL Quantum Computing Institute and the Purdue Quantum Science and Engineering Institute for support.

[1] H. N. Djidjev, G. Chapuis, G. Hahn, and G. Rizk, Efficient combinatorial optimization using quantum annealing (2018), arXiv:1801.08653 [quant-ph].

[2] K. Ikeda, Y. Nakamura, and T. S. Humble, Application of quantum annealing to nurse scheduling problem, *Scientific reports* **9**, 1 (2019).

[3] O. Titiloye and A. Crispin, Quantum annealing of the graph coloring problem, *Discrete Optimization* **8**, 376–384 (2011).

[4] H. Markowitz, Portfolio selection, *The Journal of Finance* **7**, 77 (1952).

[5] F. Black and R. B. Litterman, Asset allocation combining investor views with market equilibrium, *The Journal of Fixed Income* **1**, 7–18 (1991).

[6] S. Dasgupta and A. Banerjee, Quantum annealing algorithm for expected shortfall based dynamic asset allocation (2019), arXiv:1909.12904.

[7] A. J. McNeil, R. Frey, and P. Embrechts, *Quantitative risk management: concepts, techniques and tools-revised edition* (Princeton university press, 2015).

[8] Y. Ye and E. Tse, An extension of karmarkars projective algorithm for convex quadratic programming, *Mathematical Programming* **44**, 157–179 (1989).

[9] E. Grant, T. S. Humble, and B. Stump, Benchmarking quantum annealing controls with portfolio optimization, *Phys. Rev. Applied* **15**, 014012 (2021).

[10] E. Farhi, J. Goldstone, S. Gutmann, and M. Sipser, Quantum computation by adiabatic evolution (2000), arXiv:quant-ph/0001106.

[11] F. Barahona, On the computational complexity of ising spin glass models, *Journal of Physics A: Mathematical and General* **15**, 3241 (1982).

[12] I. D.-W. Systems, The d-wave advantage system: An overview (2021).

[13] D. Venturelli, S. Mandrà, S. Knysh, B. O’Gorman, R. Biswas, and V. Smelyanskiy, Quantum optimization of fully connected spin glasses, *Phys. Rev. X* **5**, 031040 (2015).

[14] T. Boothby, A. D. King, and A. Roy, Fast clique minor generation in chimera qubit connectivity graphs, *Quantum Information Processing* **15**, 495 (2016).

[15] G. Rosenberg, P. Haghnegahdar, P. Goddard, P. Carr, K. Wu, and M. L. de Prado, Solving the optimal trading trajectory problem using a quantum annealer, *IEEE J. Sel. Top. Signal Process.* **10**, 1053 (2016).

[16] D. Venturelli and A. Kondratyev, Reverse quantum annealing approach to portfolio optimization problems, *Quantum Mach. Intell.* **1**, 17 (2019).

[17] F. Phillipson and H. S. Bhatia, Portfolio optimisation using the d-wave quantum annealer, in *International Conference on Computational Science* (Springer, 2021) pp. 45–59.

[18] S. Uryasev and R. T. Rockafellar, Conditional value-at-risk: Optimization approach, *Applied Optimization* , 411–435 (2001).

[19] M. Norton, V. Khokhlov, and S. Uryasev, Calculating evar and bpoe for common probability distributions with application to portfolio optimization and density estima-

tion, Annals of Operations Research **299**, 1281 (2021).

[20] I. D.-W. Systems, Ice: Dynamic ranges in h and j values (2021).

[21] I. D.-W. Systems, Qpu-specific physical properties: Dw_2000q_5 (2021).

[22] E. Pelofske, G. Hahn, and H. Djidjev, Optimizing the spin reversal transform on the d-wave 2000q (2019), arXiv:1906.10955.

[23] T. Lanting, M. H. Amin, C. Baron, M. Babcock, J. Boschee, S. Boixo, V. N. Smelyanskiy, M. Foygel, and A. G. Petukhov, Probing environmental spin polarization with superconducting flux qubits (2020), arXiv:2003.14244.

[24] K. L. Pudenz, Parameter setting for quantum annealers, in *2016 IEEE High Performance Extreme Computing Conference, (HPEC)* (IEEE, 2016) pp. 1–6.

[25] H. M. Markowitz, The elimination form of the inverse and its application to linear programming, Management Science **3**, 255–269 (1957).

[26] F. Jensen, S. Lauritzen, and K. Olesen, Bayesian updating in causal probabilistic networks by local computations, Computational Statistics Quarterly **4**, 269 (1990).

[27] S. Diamond and S. P. Boyd, CVXPY: A python-embedded modeling language for convex optimization, J. Mach. Learn. Res. **17**, 83:1 (2016).

[28] A. Barbosa, E. Pelofske, G. Hahn, and H. N. Djidjev, Using machine learning for quantum annealing accuracy prediction, Algorithms **14**, 187 (2021).

[29] T. Boothby, A. D. King, and A. Roy, Fast clique minor generation in chimera qubit connectivity graphs, Quantum Inf. Process. **15**, 495 (2016).

[30] E. Farhi, J. Goldstone, and S. Gutmann, A quantum approximate optimization algorithm, arXiv preprint arXiv:1411.4028 (2014).

[31] S. Hadfield, Z. Wang, B. O’Gorman, E. Rieffel, D. Venturelli, and R. Biswas, From the quantum approximate optimization algorithm to a quantum alternating operator ansatz, Algorithms **12**, 34 (2019).